



UNIVERSITÀ POLITECNICA DELLE MARCHE  
Repository ISTITUZIONALE

The intriguing role of rhamnolipids on plasma membrane remodelling: From lipid rafts to membrane budding

This is the peer reviewed version of the following article:

*Original*

The intriguing role of rhamnolipids on plasma membrane remodelling: From lipid rafts to membrane budding / Come, B.; Donato, M.; Potenza, L. F.; Mariani, P.; Itri, R.; Spinozzi, F.. - In: JOURNAL OF COLLOID AND INTERFACE SCIENCE. - ISSN 0021-9797. - STAMPA. - 582:(2021), pp. 669-677. [10.1016/j.jcis.2020.08.027]

*Availability:*

This version is available at: 11566/286644 since: 2024-04-06T09:50:37Z

*Publisher:*

*Published*

DOI:10.1016/j.jcis.2020.08.027

*Terms of use:*

The terms and conditions for the reuse of this version of the manuscript are specified in the publishing policy. The use of copyrighted works requires the consent of the rights' holder (author or publisher). Works made available under a Creative Commons license or a Publisher's custom-made license can be used according to the terms and conditions contained therein. See editor's website for further information and terms and conditions.

This item was downloaded from IRIS Università Politecnica delle Marche (<https://iris.univpm.it>). When citing, please refer to the published version.

(Article begins on next page)

# The Intriguing Role of Rhamnolipids on Plasma Membrane Remodelling: from Lipid Rafts to Membrane Budding

Benedetta Come<sup>a</sup>, Maressa Donato<sup>b,c</sup>, Lucia Francesca Potenza<sup>a</sup>, Paolo Mariani<sup>a</sup>, Rosangela Itri<sup>b,\*</sup>, Francesco Spinozzi<sup>a,\*\*</sup>

<sup>a</sup>*Department of Life and Environmental Sciences, Polytechnic University of Marche, Italy*

<sup>b</sup>*Institute of Physics, University of São Paulo, Brazil*

<sup>c</sup>*Center for Laser and Applications, Nuclear and Energy Research Institute, São Paulo, Brazil*

---

## Abstract

Rhamnolipids (RLs) comprise a class of glycolipids produced by *Pseudomonas aeruginosa* under appropriate culture medium. They act as biosurfactants being composed by a hydrophilic head of either one (mono-RL) or two (di-RL) rhamnose moieties coupled to hydroxyaliphatic chains. It is well accepted that RLs present low biolitic activity as compared to other synthetic surfactants. However, their mechanisms of action in biological systems are not well defined yet. The interaction of RLs with lipid bilayers are here investigated to address how they impact on plasma membrane at molecular level. Our experimental approach was based on a deep analysis of optical microscopy data from giant unilamellar vesicles (GUVs) dispersed in aqueous solutions containing up to 0.5 mM of commercially available RLs (a mixture of mono-RL, 33 – 37 mol %, and di-RL, 63 – 67 mol %, *cmc* of  $0.068 \pm 0.005$  mM). GUVs were made up of a single lipid POPC and a ternary system containing DOPC, sphingomyelin and cholesterol which to mimic lipid raft platforms. Our results demonstrate that RLs have a low partition in the lipid bilayer in respect to the total molecules in solution. We suppose that RLs insert in the outer leaflet with low propensity to flip-flop. In the case of POPC GUVs, the insertion of RL molecules in the outer leaflet impairs changes in spontaneous membrane curvature with incubation time. Then, small buds are formed that remain linked to the original membrane. No changes in membrane permeability have been detected. A remarkable result refers to the insertion of RLs in membranes containing liquid ordered ( $L_o$ ) - liquid disordered ( $L_d$ ) phase coexistence. The rate of interaction has been observed to be higher for  $L_d$  phase than for  $L_o$  phase ( $0.12 \cdot 10^{-6} \text{ s}^{-1}$  and  $0.023 \cdot 10^{-6} \text{ s}^{-1}$  for  $L_d$  and  $L_o$ , respectively, at RL concentration of 0.5 mM).

---

\*Corresponding author

\*\*Corresponding author

Email addresses: f.spinozzi@univpm.it (Rosangela Itri), itri@if.usp.br (Rosangela Itri)

As a consequence, the preferential RL insertion in  $L_d$  phase may also alter the membrane spontaneous curvature which, coupled to the change in the line tension associated to the domains boundary, conducted to  $L_o$  domain protrusion. Even if it has been observed on a model system, such membrane remodelling in a model system might correlate to endocytic processes activated in cell membranes, regardless of the participation of specific proteins. Further, changes imposed by RLs in lipid rafts may affect the association of key proteins enrolled in cell signaling, which may control cell homeostasis.

*Keywords:* Membrane remodeling; lipid rafts; giant unilamellar vesicles; Rhamnolipid; biosurfactant; membrane budding; endocytosis

---

## 1. Introduction

It is well recognized that one of the biggest problems in the industrialized world is the contamination with dangerous and toxic chemicals of soil, sediments, groundwater, surface water and air [1, 2, 3]. The search of new environmental technologies includes bioremediation, which envisages the correct use of either microorganisms or microbial processes to biodegrade contaminants [4, 5]. On this ground, an increasing interest in a new class of surfactants, referred to as biosurfactants, has taken place over the last two decades. They are naturally produced by many organisms, especially by bacteria [6, 7]. Among the most investigated and exploited biosurfactants there are the glycolipids, which are carbohydrates with aliphatic or hydroxyaliphatic chains. In particular, amid glycolipids a relevant role is played by rhamnolipids (RLs), mainly produced by *Pseudomonas aeruginosa*, composed by a hydrophilic head constituted of either one (mono-RL) or two (di-RL) rhamnose moieties and one or two tails of  $\beta$ -hydroxydecanoic acids (Fig. 1), linked to a large variety of 3-(hydroxyalkanoyloxy) alkanolic acids carbon chain. Like other synthetic surfactants, RLs are able to reduce the water surface tension significantly [8, 9, 10] and to form emulsions [11]. Further, they have been successfully applied on bioremediation processes with the aim of either degrading organic waste or reducing its concentration down to the limits imposed by regulatory authorities [12]. Of note, concerning bioremediation activities in oil-contaminated waters, it has been reported that RLs can recover up to 98% of crude oil from the refractory waste, both on a laboratory scale and on pilot plants [13]. They are also effective in washing up to 95% of synthetic oil from sand [14]. RLs have been also in pharmaceuticals, cosmetics, agriculture and other industrial sectors. For instance, we have previously demonstrated that RLs can be used as epithelial permeability enhancer [8]. Besides, antiviral, antimycotic, mycoplasmacidal, algicidal and zoosporicidal activities have been reported [15, 16]. Due to the approval of the United States Environmental Protection Agency (EPA), RLs have been applied to horticultural and agricultural crops as effective biofungicides [17].

In spite of potential RLs applications, very little is known about the molecular basis of some biological actions of these biosurfactants. For instance, permeabilization and/or membrane rupture are important for biocide action. On

the other hand, for human consumption and environmental purposes, it is quite  
 35 important to correlate the RLs action mechanisms on biological membranes  
 with their molecular structures, which confer their amphipathic properties. It  
 is known that the critical micellar concentration ( $cmc$ ) of pure RLs, which form  
 micelles of circa 20 – 30 nm in size, and their mixtures is dependent on their  
 chemical composition [18, 19]. However, few studies have been dedicated to  
 40 explore the interaction between RLs, below and above  $cmc$ , and biological in-  
 terfaces at molecular level. In this regard, Ortiz and coworkers investigated  
 the effects of di-RL, which behaves as an inverted-cone shaped molecule [20, 9],  
 on the structural properties of phosphatidylcholine (PC) model membranes by  
 differential scanning calorimetry, X-Ray diffraction, fluorescence and infrared  
 45 spectroscopies [21, 22]. The combined results revealed that di-RL intercalates  
 in the PC bilayers promoting an increase in phospholipid hydrocarbon chain  
 disorder. This process perturbs the packing of PC molecules emphasized by  
 the reduction of cooperativity in the gel to liquid crystalline phase transition.  
 Further, di-RL induces leakage of carboxyfluorescein (CF) entrapped into POPC  
 50 unilamellar vesicles [23]. Interestingly, the presence of a lag period was evident  
 for all di-RL concentrations below  $cmc$  of 0.11 mM, being shorter for increas-  
 ing di-RL concentration. Such CF leakage was not accompanied by membrane  
 disruption. On the contrary, at di-RL concentrations above  $cmc$ , POPC bilayer  
 displays a quick CF-leakage concomitantly with membrane solubilization. Of  
 55 note, the presence of phosphatidylethanolamine, a cone-shaped lipid, inhibits  
 the effect of di-RL in POPC membranes due to favoured lipid packing [20, 23].  
 In addition, cholesterol exhibits a protective action against membrane perme-  
 abilization [23]. Such findings could be of particular interest because plasma  
 membrane of eukaryotic cells can contain up to 50 mol % of cholesterol, which  
 60 would protect the human cells from di-RL damage in a first insight.

Interestingly, Ortiz and coworkers [23] also investigated the impact of di-RL  
 on red blood cells used as model cells. The authors have demonstrated that  
 di-RLs at concentrations below  $cmc$  are able to promote human erythrocytes  
 permeabilization via detergent-like mechanism. In parallel, electron microscopy  
 65 images have revealed alterations of red blood cell morphology from usual bi-  
 concave disk-like shape to swollen cells (spherocytes), some of them presenting  
 protrusions on cell surface (echinocytes). Such morphological changes must in-  
 dicate either a di-RL preferential partition into the outer plasma membrane or  
 alterations in the cytoskeleton [23]. Of note, a small lag period has been ob-  
 70 served for all studied di-RL concentrations below  $cmc$ , indicating that an initial  
 di-RL interaction mechanism upon the cells takes place prior to erythrocytes  
 hemolysis. Such mechanism of interaction remains yet obscure in the literature.

Regarding *in-vivo* assays, the impact of RL against a phagotropic alga  
*Ochromonas danica* has been recently reported [24]. Interestingly, such alga  
 75 species represents a group of phagotropic flagellates ecologically important for  
 aquatic systems, with no protective cell wall. In this case, biolitic and permeabil-  
 ity effects on the algal plasma membrane are only observed at RL concentrations  
 above  $cmc$ , unlike the impact of synthetic surfactants as sodium dodecyl sul-  
 fate (SDS) that occurs at sub-micellar concentrations. It means that whereas

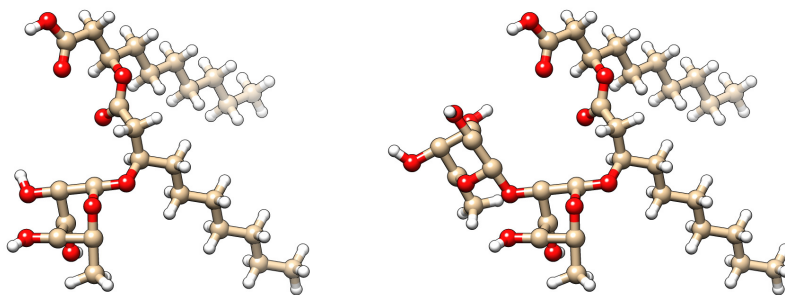


Figure 1: Ball-and-stick representations of a mono-RL (RL - C<sub>10</sub> - C<sub>10</sub>, left) and a di-RL (RL - RL - C<sub>10</sub> - C<sub>10</sub>, right).

individual SDS molecules are able to damage *O. danica* cell membrane probably forming mixed micelles with membrane lipids, RLs must preferentially interact with the plasma membrane just when micelles are formed in solution. Also, RL-induced motility loss was identified [24].

Therefore, although several preceding works have addressed the influence of the biosurfactant RL on biomembranes, its mechanism of action on plasma membrane at molecular level remains elusive. It should bear in mind that plasma membrane lipid composition is close to a critical point of phase separation [25]. From the biological point of view, being close to a critical point the cell requires much less energy to promote lipid demixing and to create lipid heterogeneity known as lipid rafts. Such rafts platforms mediate protein-protein and protein-membrane interactions that are the key actors in cell signalling processes [26, 27, 28, 25]. In this light, here we investigate the effect of a commercially available RL mixture composed of mono-RL (33–37 mol %) and di-RL (63–67 mol %) [8] on plasma membrane models represented by giant unilamellar vesicles (GUVs) above *cmc*. Two types of GUVs were challenged by the RL mixture for comparison purposes and observed under an optical microscopy in both phase contrast and fluorescence modes. They were: GUVs made up of a single lipid, POPC, and of a ternary mixture of DOPC, sphingomyelin (SM) and cholesterol (CHOL), at molar ratio 1:1:1, which present liquid-ordered (L<sub>o</sub>) liquid-disordered (L<sub>d</sub>) phase coexistence [29] resembling lipid rafts [29]. In this way, changes in lipid rafts organization, membrane remodelling, permeabilization and membrane disruption elicited by RLs can be simultaneously evaluated by optical microscopy. Such experimental procedure allows us to describe the RLs action mechanisms underlining the plasma membrane response, as follows.

## 2. Materials and methods

### Sample preparation

RL from *Pseudomonas Aeruginosa* (powder, 90% purity) was purchased from Sigma-Aldrich (Poole, UK). As described by Perinelli et al. [8], this commercial product is mainly composed by a mixture of mono-rhamnolipids (33 –

110 37 mol %) and di-rhamnolipids (63 – 67 mol %) and the *cmc* in water was estimated as 0.16 mM.

Herein, RL will be dispersed in glucose solution as described below. Accordingly, *cmc* was determined by surface tension and amounted to  $0.068 \pm 0.005$  mM (Fig. S1).

115 All studied lipids were acquired from Sigma-Aldrich: POPC (2-oleoyl-1-palmitoyl-*sn*-glycero-3-phosphocholine), DOPC (1,2-di(*cis*-9-octadecenoyl)-*sn*-glycero-3-phosphocholine), sphingomyelin (SM, N-acyl-4-sphingenyl-1-O-phosphorylcholine, N-Acyl-D-sphingosine-1-phosphocholine), cholesterol (CHOL, 3 $\beta$ -hydroxy-5-cholestene, 5-cholesten-3 $\beta$ -ol) and DOPE (1,2-dioleoyl-*sn*-glycero-3-phosphoethanolamine)-rhodamine, Rho-PE. All other chemicals and solvents were purchased from  
120 Sigma Aldrich (Saint Louis, MO) and used without further purification.

GUVs were prepared by the electroformation procedure using POPC, POPC/Rho-PE (0.1 mol %) and DOPC, SM, CHOL (molar ratio 1:1:1) containing Rho-PE (0.1 mol %). Briefly, 20  $\mu$ L of 1.0 g/L total lipid in chloroform solution were  
125 spread on the surfaces of two conductive glass slides coated with indium tin oxide (ITO slides, Sigma-Aldrich, Saint Louis, MO). The glass slides were placed with their conductive sides facing each other and separated by a 2 mm thick Teflon frame. The chamber was filled with a 0.2 M sucrose solution up to a volume of 1.0 mL. The glass plates were connected to a function generator  
130 applying an alternating voltage of 2 V with 10 Hz frequency for 2 h. The electroformation of GUVs composed of DOPC:SM:CHOL was conducted at 55° C. These GUVs were left at 4° C overnight and observed in the following day. Subsequently, 100  $\mu$ L of electroformed GUVs were mixed to 600  $\mu$ L of a 0.2 M glucose solution containing RL and immediately transferred to the microscope  
135 chamber to perform continuous observations. The final total lipid concentration was 0.00286 g/L, whereas the RL concentration ranged from 0.1 mM to 0.5 mM. The osmolarities of the sucrose and glucose solutions were measured with a cryoscopic osmometer Osmomat 030 (Gonotec, Germany) and carefully matched to avoid osmotic pressure effects thus guaranteeing the optical contrast.  
140 Experiments were done at least in triplicate.

#### *Microscope observations*

Vesicles were observed in the phase contrast and fluorescence modes by means of an inverted microscope Axiovert 200 (Carl Zeiss, Jena, Germany) equipped with a Plan Neo-Fluar 63X Ph2 objective (NA 0.75). Images were  
145 recorded with an AxioCam HSm digital camera (Carl Zeiss). A mercury lamp HBO 103 W, with excitation and emission filters at 540 – 552 nm and 575 – 640 nm, respectively, was used in the fluorescence mode. The effect of lipid oxidation was controlled by the use of low intensity illumination in the fluorescence microscopy to avoid artifacts due to light-induced domain formation by  
150 the Rho-probe [30, 31]. All measurements were done at  $(23 \pm 2)^\circ$  C.

#### *Data analysis*

Several hundreds of snapshots of the GUVs, collected as a function of time after the mixing with a glucose solution at different RL concentration, were

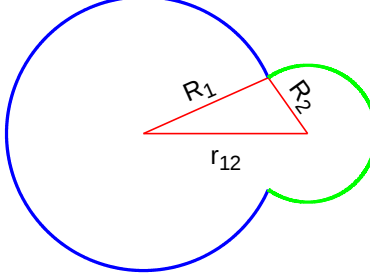


Figure 2: Projection into the plan of a vesicle formed by sealing a vesicle of radius  $R_1$  with a vesicle of radius  $R_2$ , being  $r_{12}$  the distance between the centers of the two vesicles. Blue and green arcs refer to  $A_1$  and  $A_2$  surfaces, respectively.

analyzed by using original macros that we have developed under the ImageJ software [32].

GUVs formed by POPC appear approximately as circles when observed with the microscope, indicating that their shape is almost spherical. By a set of user-selected points placed over the border of a POPC GUV microscopy snapshot, a first ImageJ macro allows to calculate the coordinates of the center and the radius  $R$  of the best circle passing among the points (see Fig. S2 in the SI), corresponding to the radius of the spherical vesicle, together with their standard deviations. Details are shown in Sec. S2 of the SI.

On the other side, the shape of GUVs constituted by DOPC:SM:CHOL, observed with the microscope as a function of the time after the interaction with RL, appears as a combination of two spherical caps [33], as shown in Fig. 2. To note, we have considered, among the GUVs formed by two spherical caps, only the ones that, during the observation time, appear to maintain the line joining the two spherical caps centers almost parallel to the observation plane. In this cases, in order to estimate the radii of the two spherical caps,  $R_1$  and  $R_2$  (assuming  $R_1 \geq R_2$ ), and the distance  $r_{12}$  between their centers, together with their standard deviations, a second ImageJ macro has been developed, which requires the user to select two sets of points over the border, respectively, of the two circular arcs that appear in the microscope snapshot. The equations exploited by this ImageJ macro are detailed in Sec. S3 of the SI.

The surfaces of the two spherical caps with radius  $R_1$  and  $R_2$ , respectively, are given by the following expressions [33]

$$A_1 = \frac{\pi R_1}{r_{12}} (R_1^2 - R_2^2 + r_{12}(r_{12} + 2R_1)) \quad (1)$$

$$A_2 = \frac{\pi R_2}{r_{12}} (R_2^2 - R_1^2 + r_{12}(r_{12} + 2R_2)) \quad (2)$$

The total surface of the two sealed spherical caps vesicle is clearly  $A = A_1 + A_2$ ,

whereas the enclosed volume of the whole vesicle is calculated according to

$$V = \frac{\pi}{12r_{12}}(R_1 + R_2 + r_{12})^2(3R_1^2 + 2R_1r_{12} - r_{12}^2 - 6R_1R_2 + 2r_{12}R_2 + 3R_2^2) \quad (3)$$

Equations exploited to calculate the standard deviations of surface areas ( $A_1$ ,  $A_2$  and  $A$ ) and volume  $V$  are reported in Sec. S3 of the SI.

### 3. Results and discussion

In order to investigate the interaction between RLs and mimetic phospholipid plasma membranes, we initially considered homogeneous POPC GUVs exposed to the biosurfactants. Spherical vesicles dispersed in 0.1 mM RL-containing glucose solution (i.e. above *cmc*) do not present any morphological alteration and preserve their optical contrast over approximately 1000 s of continuous observation. It means that, at such concentration, RLs did not cause membrane permeabilization, which would be characterized by sugar exchange between the inner and outer GUVs compartments. Such finding apparently contrasts with those reported by Sánchez et al. [23], where the authors have evidenced 100% of CF release from POPC LUVs interacting with 0.1 mM di-RL (near its *cmc* of 0.11 mM in water) in an elapsed time of 600 s, with no membrane solubilization. It should be remarked, however, that here we investigate POPC GUVs incubated in a solution containing 0.1 mM of a mixture of mono and di-RLs, relatively close to the *cmc* value of  $0.068 \pm 0.005$  mM in glucose solution (Fig. S1.) Further, the GUVs membrane curvature could also hinder the inverted-cone shaped RLs molecules insertion into POPC bilayers in respect to LUVs, thus justifying the differences found in membrane permeabilization data.

Fig. 3 shows typical morphological changes imposed by submitting POPC GUVs to increasing RL concentrations. At 0.2 mM RL (*circa* 3-fold the *cmc*) the membrane suffers only subtle fluctuations with the emission of few small buds (small micro-sized vesicles linked to the original GUV, Fig. 3, panel A), preserving the original membrane surface area over time (Fig. 4, green circles). This was accounted for by evaluating, with the first ImageJ macro (see Sec. “Data analysis”), the radius of a circle surrounding the GUV spherical shape (Fig. 3, panel B).

On the other hand, in the case of POPC bilayers dispersed in 0.5 mM RL containing outer solution, RL promotes marked GUVs fluctuations (Fig. 3, panels C and D) accompanied by significant area increase after *circa* 600 s of membrane:RL contact (maximum at 634 s, Fig. 4, red circles). This indicates that RL molecules inserted in the membrane produces an excess of surface area. As response, the membrane emits buds (highlighted as fluorescent small GUVs linked to the original one, Fig. 3, panel C, fluorescence mode) to release the area excess returning to its original area. In this way, both the lipid bilayer forming the bud and the surrounding membrane matrix are in fluid state. Then, phospholipid molecules can flow and rearrange themselves within the plane of

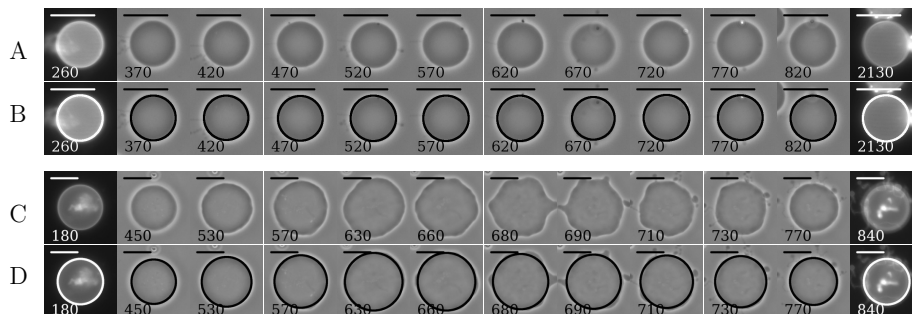


Figure 3: Representative GUV fluorescence images (the first and last ones of each row) and phase contrast images of POPC (0.00376 mM) with 0.1 mol % Rho-PE dispersed in 0.2 mM RL (panel A) and 0.5 mM RL-containing glucose solution (panel C). The time sequence, expressed in seconds in the bottom left corner of each image, refers to the elapsed time after mixing RL with GUV solution (considered as time 0 s). The images of panels A and C with superimposed the best circle surrounding the GUVs determined with the first ImageJ macro are reported in panels B and D, respectively. The top right bars span 20  $\mu\text{m}$ .

the membranes [34]. Of note, due to RLs bulky molecular structure (Fig. 1) we suggest that they must be mainly located in the outer leaflet of the membrane with no or very slow flip-flop. Interestingly, we calculate the ratio of RL bound to the outer leaflet in respect to the POPC lipid based on the POPC GUV area increase (Fig. 4). This ratio amounted to  $0.092 \pm 0.004$  at maximum area increase (Eq. S32). Further, the time evolution of the fraction of GUV-bound RL in respect to total RL added to the outer solution resulted to be  $(4.3 \pm 0.2) \cdot 10^{-6} \text{ s}^{-1}$  (Eq. S36 with  $\zeta_d = 116$ ). Therefore, the RL partition in POPC is low, even tough it is able to promote increase in membrane area, followed by buds protusion. No changes in membrane permeability have been detected under RL influence, since no optical contrast fade has been observed. So, packing defects, which could lead to observable GUV leakage, were not evidenced in these experiments. Moreover, neither membrane solubilization nor rupture have been registered in the elapsed time of  $\approx 1000 \text{ s}$ , unlike the deleterious effects previously demonstrated by synthetic surfactants as SDS and Triton-X on POPC GUVs [35, 36, 37, 38].

In the following, we present the optical microscopy results regarding the impact of RLs on GUVs presenting  $L_o$ - $L_d$  phase coexistence. The heterogeneous vesicles were made of equimolar contents of DOPC:SM:CHOL at the concentration 0.00286 g/L (corresponding to 0.00431 mM of total lipids molecules) and 0.1 mol % of Rho-PE. Fig. 5, panels A and C, shows representative GUVs images exposed to 0.2 mM RL and 0.5 mM RL, respectively.

It is well known that  $L_d$ - $L_o$  phase coexistence is easily recognized by fluorescence microscopy since the fluorescent probe Rho-PE prefers to partition in  $L_d$  phase [29]. In this way, Fig. 5 displays an initial dark liquid ordered  $L_o$  domain within a bright liquid disordered  $L_d$  phase in a spherical GUV. Interestingly, as time evolves, RL-induced membrane remodeling gradually takes place resulting

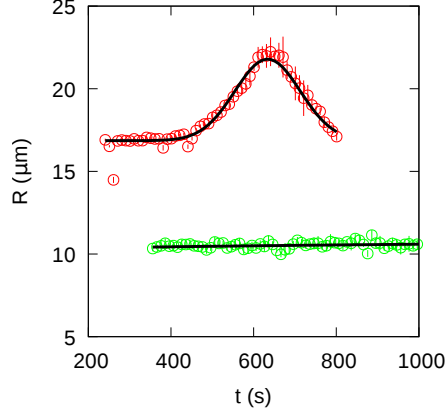


Figure 4: Time-dependence of the radius of POPC GUV in the presence of 0.2 mM (green circles) and 0.5 mM (red circles) RL. The black line represents the best fit to the data using a Gaussian function over a flat background. Fitting parameters for GUVs interacting with 0.5 mM RL are: background  $(16.857 \pm 0.004) \mu\text{m}$ , height  $(4.9 \pm 0.3) \mu\text{m}$ , standard deviation  $(79 \pm 3) \text{ s}$ , peak position  $(634 \pm 3) \text{ s}$ .

into  $L_o$  phase outward budding. Note that  $L_o$  phase protrusion is faster for increasing RL amount. It should be noted that experiments in the absence of RL were carried out as control and no alterations in the original GUVs were observed.

Herein we analyse such morphological change by taking into account two circles of radii  $R_1$  (left side) and  $R_2$  (right side) that encompass the GUV (Fig. 2), related to the displacement of  $L_d$  phase in respect to the  $L_o$  phase, respectively, together with the distance  $r_{12}$  between their centres. Best circles and center-to-center distances, obtained through the second ImageJ macro as described in Sec. “Data analysis”, are superimposed to the microscope images in Fig. 5, panel B, for 0.2 mM RL and panel D for 0.5 mM RL. Corresponding values of  $R_1$ ,  $R_2$  and  $r_{12}$  are plotted as a function of the time in Fig. 6, panels A and B, whereas the values of the total GUV surface  $A$  are displayed in panel C, of the  $L_d$  and  $L_o$  surfaces  $A_1$  and  $A_2$ , calculated with Eqs. 1-2, respectively, in panels D and E, and of GUV volume  $V$  in panel F. To note, also the values obtained by the microscope observations of the control DOPC:SM:CHOL GUVs in the absence of RL are shown.

Both the time evolution of circles’ radii  $R_i$  ( $i = 1, 2$ ) as well as the distance  $r_{12}$  between the centres of the circles have been approximated with the following sigmoidal behaviours,

$$R_i(t) = R_i^0 + (R_i^\infty - R_i^0) \frac{1 - \exp\left(-\frac{t}{\Delta t_{R_i}}\right)}{2 - \exp\left(-\frac{t}{\Delta t_{R_i}}\right) - \exp\left(-\frac{t_{0,R_i}}{\Delta t_{R_i}}\right)} \quad (4)$$

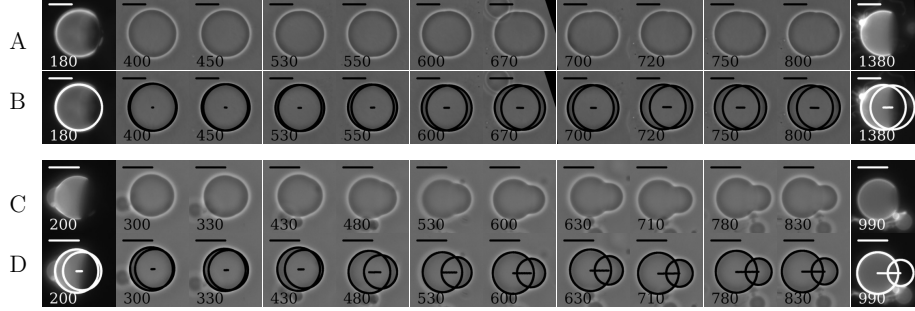


Figure 5: Representative fluorescence images (the first and last ones of each row) and phase contrast images of a GUV composed by DOPC, SM, CHOL (1:1:1) (at 0.00431 mM total lipid concentration) and 0.1 mol % Rho-PE dispersed in a glucose solution containing 0.2 mM RL (panel A) and 0.5 mM RL (panel C). The time sequence, expressed in seconds in the bottom left corner of each image, refers to the elapsed time after mixing RL with GUV solution (considered as time 0 s). The images of panels A and C with superimposed the best two circles surrounding the GUVs determined with the second ImageJ macro are reported in panels B and D, respectively. All images have been rotated in order to get the line connecting the centres of the two circles (shown in panels B and D) in the horizontal direction, with the large and the small circle, of radius  $R_1$  and  $R_2$ , on the left and the right side, respectively (Fig. 2). The distance  $r_{12}$  (Eq. 5) between the centres (Fig. 2) is shown as black or a white line. The top right bars span 20  $\mu\text{m}$ .

$$r_{12}(t) = r_{12}^{\infty} \frac{1 - \exp\left(\frac{t}{\Delta t_{r_{12}}}\right)}{2 - \exp\left(\frac{t}{\Delta t_{r_{12}}}\right) - \exp\left(\frac{t_{0,r_{12}}}{\Delta t_{r_{12}}}\right)} \quad (5)$$

where  $R_i^0$  represents the value at the beginning ( $t = 0$ ),  $R_i^{\infty}$  or  $r_{12}^{\infty}$  are the values at the plateau (when the time  $t$  tends to infinity),  $t_{0,R_i}$  or  $t_{0,r_{12}}$  are the time values in the middle of the transition and  $\Delta t_{R_i}$  or  $\Delta t_{r_{12}}$  corresponds to the time widths at the transition.

Fitting parameters obtained by applying those approximations are reported in Table 1. The time trends of the total and the partial GUV surfaces ( $A$ ,  $A_1$  and  $A_2$ ), as well as the ones of the GUV volumes  $V$  result to be almost linear, as shown by the best fitting straight lines reported in Fig. 6, panels C-F. The corresponding slopes ( $m_A$ ,  $m_{A_1}$ ,  $m_{A_2}$  and  $m_V$ ) and intercepts at  $t = 0$  ( $A_0$ ,  $A_{1,0}$ ,  $A_{2,0}$  and  $V_0$ ) are shown in Table 1.

Results indicate that, for 0.2 mM RL, whereas both radii attributed to the disordered and the ordered phases ( $R_1$  and  $R_2$ , respectively) are quite similar and slightly decrease of *circa* 6% over time (Fig. 6, panel A, open and closed circles, respectively, and Table 1), the distance  $r_{12}$  between their centres changes of *circa* 6  $\mu\text{m}$  in an elapsed time of 1000 s of RL-heterogeneous GUV contact, with a mid transition time  $t_{0,r_{12}} \approx 540$  s (Fig. 6, panel B, circles and Table 1). Such transition is accompanied by a tiny increase in the comprised area (Fig. 6, panel C (circles) and Table 1: the slope is  $m_A \approx 0.3 \mu\text{m}^2\text{s}^{-1}$ , corresponding to a relative variation from 180 to 1000 s in the order of 4%), while the volume

remains almost unaltered (Fig. 6, panel F (triangles) and Table 1. From one hand, the constancy of the volume confirms that during the observation time the line joining the two spherical cap centers remains almost parallel to the microscope observation plane, confirming the goodness of the present analysis method. From the other hand, it is worth to notice that the main contribution to the increase of  $A$  derives from  $A_1$ , revealing that the most important effect of 0.2 mM RL in the plasma membrane mimetic is its insertion in the  $L_d$  phase.

A remarkable result was observed by increasing the RL amount to 0.5 mM. During the RL:membrane interaction, the original GUV practically maintains its radius ( $R_1^0 \approx R_1^\infty \approx 14 \mu\text{m}$ , Fig. 6, panel A, open triangles, and Table 1) whereas the protuded membrane presents a decreasing in size over time ( $R_2$  decreases from  $\approx 14 \mu\text{m}$  to  $\approx 9 \mu\text{m}$ , Fig. 6, panel A, close triangles, and Table 1). The distance  $r_{12}$  between the centres of vesicles extends up to *circa*  $16 \mu\text{m}$  and the mid-time transition is  $t_{0,r_{12}} \approx 490 \text{ s}$  in very good agreement with  $t_{0,R_2}$ , the mid-time transition of  $R_2$  (Fig. 6, panel B (triangles), Table 1). Such membrane remodelling is accompanied by an important total area increase (Fig. 6, panel C, triangles, and Table 1): the slope  $m_A$  is  $\approx 0.5 \mu\text{m}^2\text{s}^{-1}$ , corresponding to a relative variation from 180 to 1000 s in the order of 16%) and much less important volume increase (Fig. 6, panel F, triangles, and Table 1: the slope  $m_V$  is  $\approx 1 \mu\text{m}^3\text{s}^{-1}$ , corresponding to a relative variation from 180 to 1000 s in the order of 6%). To note, most of the variation of  $A$  is due to the increase of  $A_1$  ( $m_{A_1} \approx m_A$  and  $m_{A_2} \approx 0$ , Table 1), thus confirming that the biosurfactant RL mostly interacts with the  $L_d$  phase.

In a interesting matter, the fraction of RL molecules into the outer membrane in regard to the total biosurfactants in solution can be derived from the linear increasing of the surface areas  $A_1$  and  $A_2$  from  $L_d$  and  $L_o$  domains, as a function of time, according to  $f_d = \gamma_d t$  and  $f_o = \gamma_o t$ , respectively. Details of this derivation are fully described in Sec. S4 of the SI. To note, the constant rates of interaction,  $\gamma_d$  and  $\gamma_o$ , are related to the linear fitting parameters of the surfaces  $A_1$  and  $A_2$  (see Eqs. S36 and S37 of the SI).

By assuming that the area per polar head of the DOPC, SM, CHOL lipids are, respectively,  $a_{\text{DOPC}} = 64 \text{ \AA}^2$ ,  $a_{\text{SM}} = 45 \text{ \AA}^2$ ,  $a_{\text{CHOL}} = 27 \text{ \AA}^2$  and that the one of RL, derived by SAXS [39], is  $a_{\text{RL}} = 200 \text{ \AA}^2$ , we have obtained the values of  $\gamma_d$  and  $\gamma_o$  shown in the bottom lines of Table 1. As expected,  $\gamma_d$  is always greater than  $\gamma_o$  and both parameters increase with the RL amount in solution.

Results of this analysis deserve some comments. For example, at 0.2 mM RL, after 180 s of RL:membrane interaction, the fraction of RL in the disordered domain is  $f_d = (1.9 \pm 0.2) \cdot 10^{-5}$  and the one in the ordered domain results basically zero, within the experimental error ( $f_o = (0.0 \pm 0.2) \cdot 10^{-5}$ ). After 1000 s, the maximum time under microscope GUV observations, our results show an increase of  $f_d$  to  $(10 \pm 1) \cdot 10^{-5}$  without significant modification of  $f_o$  ( $f_o = (0 \pm 1) \cdot 10^{-5}$ ). This finding demonstrates that RLs at this concentration interact preferentially with liquid disordered domain in the experiment time-course. Note that the partition is relatively low in the membrane in respect to the solution.

Completely different is the landscape at 0.5 mM RL. Indeed, after 180 s from

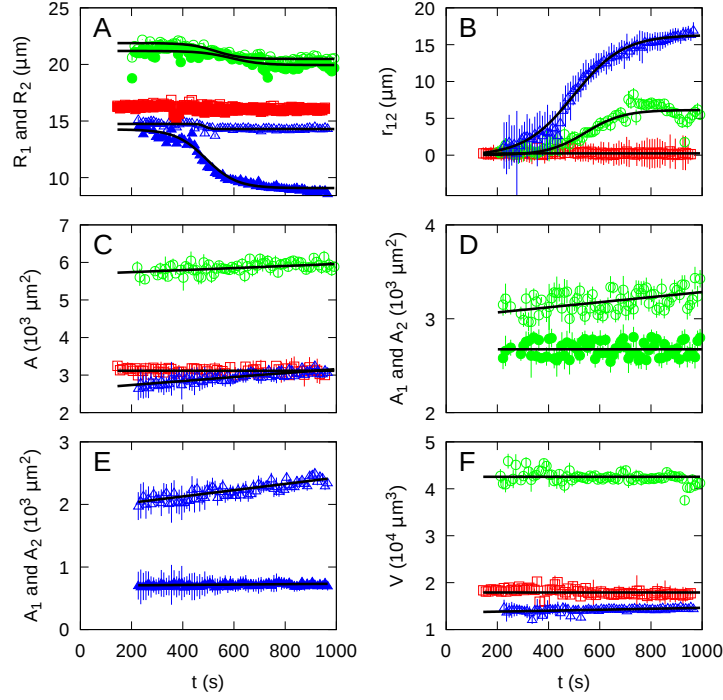


Figure 6: Time-dependence of the geometrical parameters of the GUVs formed by DOPC, SM, CHOL (1:1:1) in the absence of RL (red squares) and in the presence of 0.20 and 0.50 mM RL (green circles and blue triangles, respectively). Panel A: large ( $R_1$ , open symbols) and small ( $R_2$ , filled symbols) circle radius and best fitting obtained with sigmoidal function (Eq. 4). Panel B: centre-to-centre distances and best fitting obtained with sigmoidal function (Eq. 5). Panel C: total surface of the GUVs and best fitting obtained with straight lines. Panels D: surfaces  $A_1$  (open green circles) and  $A_2$  (closed green circles) of the spherical caps with radius  $R_1$  and  $R_2$  in the presence of 0.20 mM RL and best fitting obtained with straight lines. Panels E: surfaces  $A_1$  (open blue triangles) and  $A_2$  (closed blue triangles) of the spherical caps with radius  $R_1$  and  $R_2$  in the presence of 0.50 mM RL and best fitting obtained with straight lines. Panel F: volume of GUVs and best fitting obtained with straight lines.

| [RL]                | (mM)                                      | 0.00            | 0.20             | 0.50              |
|---------------------|---|-----------------|------------------|-------------------|
| $R_1^0$             | ( $\mu\text{m}$ )                         | —               | $21.88 \pm 0.06$ | $14.74 \pm 0.03$  |
| $R_1^\infty$        | ( $\mu\text{m}$ )                         | —               | $20.49 \pm 0.03$ | $14.29 \pm 0.02$  |
| $t_{0,R_1}$         | (s)                                       | —               | $527 \pm 6$      | $490 \pm 10$      |
| $\Delta t_{R_1}$    | (s)                                       | —               | $50 \pm 10$      | $11 \pm 9$        |
| $R_2^0$             | ( $\mu\text{m}$ )                         | —               | $21.2 \pm 0.1$   | $14.25 \pm 0.09$  |
| $R_2^\infty$        | ( $\mu\text{m}$ )                         | —               | $19.95 \pm 0.06$ | $9.07 \pm 0.06$   |
| $t_{0,R_2}$         | (s)                                       | —               | $590 \pm 20$     | $491 \pm 5$       |
| $\Delta t_{R_2}$    | (s)                                       | —               | $60 \pm 20$      | $60 \pm 4$        |
| $r_{12}^\infty$     | ( $\mu\text{m}$ )                         | —               | $6.1 \pm 0.2$    | $16.3 \pm 0.1$    |
| $t_{0,r_{12}}$      | (s)                                       | —               | $540 \pm 10$     | $499 \pm 3$       |
| $\Delta t_{r_{12}}$ | (s)                                       | —               | $74 \pm 10$      | $96 \pm 3$        |
| $m_A$               | ( $10^{-2} \mu\text{m}^2 \text{s}^{-1}$ ) | $0 \pm 4$       | $27 \pm 4$       | $53 \pm 4$        |
| $A_0$               | ( $10^3 \mu\text{m}^2$ )                  | $3.11 \pm 0.03$ | $5.69 \pm 0.03$  | $2.63 \pm 0.02$   |
| $m_{A_1}$           | ( $10^{-2} \mu\text{m}^2 \text{s}^{-1}$ ) | —               | $27 \pm 3$       | $50 \pm 4$        |
| $A_{1,0}$           | ( $10^3 \mu\text{m}^2$ )                  | —               | $3.01 \pm 0.02$  | $1.93 \pm 0.02$   |
| $m_{A_2}$           | ( $10^{-2} \mu\text{m}^2 \text{s}^{-1}$ ) | —               | $0 \pm 2$        | $3 \pm 1$         |
| $A_{2,0}$           | ( $10^3 \mu\text{m}^2$ )                  | —               | $2.67 \pm 0.02$  | $0.701 \pm 0.007$ |
| $m_V$               | ( $\mu\text{m}^3 \text{s}^{-1}$ )         | $0.0 \pm 0.3$   | $0.0 \pm 0.6$    | $1.0 \pm 0.2$     |
| $V_0$               | ( $10^4 \mu\text{m}^3$ )                  | $1.79 \pm 0.02$ | $4.26 \pm 0.04$  | $1.36 \pm 0.01$   |
| $\gamma_d$          | ( $10^{-6} \text{s}^{-1}$ )               | —               | $0.10 \pm 0.01$  | $0.12 \pm 0.01$   |
| $\gamma_o$          | ( $10^{-6} \text{s}^{-1}$ )               | —               | $0.00 \pm 0.01$  | $0.023 \pm 0.008$ |

Table 1: Fitting parameters of time-depending geometrical features of GUVs formed by DOPC, SM, CHOL (1:1:1) at different RL concentrations. Parameters  $R_i^0$ ,  $R_i^\infty$ ,  $t_{0,R_i}$  and  $\Delta t_{R_i}$  (with  $i = 1, 2$ ) regard the sigmoidal approximations (Eq. 4) representing the trend of the radii shown in Fig. 5, panel A. Parameters  $r_{12}^\infty$ ,  $t_{0,r_{12}}$  and  $\Delta t_{r_{12}}$  regard the sigmoidal curves (Eq. 5) representing the trend of the centre-to-centre distance shown in Fig. 5, panel B. Slopes of the straight lines representing the trend of the total area  $A$ , the  $L_d$  and  $L_o$  areas  $A_1$  and  $A_2$ , respectively, and volume  $V$  of the GUVs (Fig. 6, panels C-F) are parameters  $m_A$ ,  $m_{A_1}$ ,  $m_{A_2}$  and  $m_V$ , respectively. Corresponding intercepts are  $A_0$ ,  $A_{1,0}$ ,  $A_{2,0}$  and  $V_0$ , respectively. Rates of the fractions of RL molecules interacting with  $L_d$  or  $L_o$  are  $\gamma_d$  and  $\gamma_o$  (Eqs. S36 and S37 of the SI), respectively.

the beginning of the interaction, the two fractions are  $f_d = (2.2 \pm 0.2) \cdot 10^{-5}$  and  $f_o = (0.4 \pm 0.2) \cdot 10^{-5}$ , indicating that a not negligible amount of RL also interacts with the ordered domain. Moreover, after 1000 s, the two fractions increase to  $f_d = (12 \pm 1) \cdot 10^{-5}$  and  $f_o = (2.3 \pm 0.8) \cdot 10^{-5}$ . Interestingly, we also observe some scenarios where Rho-PE molecules can be found in the budding region (fluorescence mode) of the membrane after longer period of RL-GUV contact (Fig. S3 of the SI). This means that the presence of RL in the lipid bilayer may either fluidify the ordered phase or promote a sort of lipid lateral rearrangement thus conducting to a less ordered phase in the budding region.

It is worth remarking that the presence of  $L_o$  domain *per se* is not enough for budding process (see results displayed on Fig. 6 from GUVs in the absence of RL (squares)). On the other hand, the RL interaction with the outer lipid bilayer triggers budding at the  $L_o$  domain site. Supposing that the rate of

RL flip-flop is slow, the budding may be partially driven due to alteration of the membrane local spontaneous curvature. This because an area difference between the two monolayers arises due to RL insertion [34]. A budding process  
345 may thus take place because it allows for increasing the outside/inside surface ratio of the two leaflets. In addition, as the  $L_d$  phase surface area increased due to preferential RL partition in respect to that of  $L_o$  phase, the excess free energy associated to the boundary line between the two phases should increase [34, 40]. As membrane response,  $L_o$  budding occurs which favors line energy reduction.  
350 In fact, the distance  $r_{12}$  between the two domains increased, concomitantly with the decrease in  $R_2$  radius (Fig. 5, panels C and D, and Fig. 6, panels A and B), resulting in a decrease of the boundary between  $L_d$  and  $L_o$  phases. Noticeable, we also observed the progression of  $L_d - L_o$  domains separation after long RL-GUV incubation time (Fig. S3 of the SI): a tiny neck joining the two domains  
355 took place, which reduced significantly the line energy (practically abolishing).

Budding has also been previously observed on POPC:SM:CHOL GUVs induced by sub-*cmc* concentration of Triton-X in less than 10 s of detergent incubation, followed by membrane fission [41]. Here we did not detect fission produced by RL on the lipid bilayers. More recently it has been shown that  
360 Triton-X has the ability to rearrange lateral heterogeneity of POPC:SM:CHOL mixtures with selective solubilisation [42]. We should bear in mind that mono and di-RLs, although amphipathic, are bulkier molecules than Triton-X which must hinder their flip-flop to the inner membrane leaflet. As a consequence, lipid bilayer solubilization is precluded, unlike the effects of others synthetic  
365 surfactants that are able to translocate to the inner layer [36, 37, 38].

Membrane budding of ordered domain has also been reported for other amphipathic molecules as non-ionic detergents, SDS, lyso-PC [43] and a sort of cell-penetrating peptides on cell membranes [44]. In particular, as revealed here, the molecules' partition is preferentially into the  $L_d$  phase-containing outer leaflet  
370 (even if initially). Therefore, the RL-induced budding mechanism in the inhomogenous GUVs studied, which display lipid-rafts platforms, seems to be a more general rule driven by lipidic forces. Interestingly, it has been shown that changes in membrane curvature towards budding activate massive endocytosis process independent of specific proteins [45]. Here we have demonstrated that  
375 the biosurfactant RL, at concentrations above *cmc*, impacts on plasma membrane models and promotes membrane remodelling towards  $L_o$  domain budding. Such mechanism may correlate to the endocytosis activation process reported in cells for other amphipathic compounds [43] as well as it may affect the function of specific biomolecules enrolled in lipid rafts. It is worth remarking that,  
380 even though RLs can be considered less toxic than usual synthetic surfactants in terms of membrane disruption and/or pores' formation, they can interfere severely in cell homeostasis through lipid membrane remodelling.

#### 4. Concluding Remarks

It is well known that rhamnolipids have been used in a large variety of  
385 applications as environment bioremediation, biomedicines, foods and cosmet-

ics [46]. However, the concentration-dependent RLs damage at cellular level is still poorly understood. In the current work, we describe the interaction of RLs with plasma membrane models. Our results clearly evidenced the RL molecules insert in the model membrane with no lytic effect for concentrations ranging from 0.1 mM to 0.5 mM (*cmc* of  $0.068 \pm 0.005$  mM in glucose solution). Nevertheless, they are able to promote membrane remodelling. As a consequence, membrane remodelling takes place. In the case of POPC GUVs, the insertion of RL molecules with time promotes a gradual increase in GUV area until a maximum value was reached (Fig. 4). The GUV restores its original area by releasing the area excess and lateral tension through the formation of small buds that remain linked to the original membrane. Strikingly, RLs on GUVs composed of DOPC:SM:CHOL, that display  $L_o$ - $L_d$  lateral phase separation as rafts platforms, drive  $L_o$  domain budding in a micro-scale. Interestingly, our data analysis gives support to conclude that RLs preferentially partition in the  $L_d$  phase (at least initially), as highlighted by the values of  $A_1$  and  $A_2$  as well as by the interaction rates  $\gamma_d$  and  $\gamma_o$ .

Of note, the increase propensity of the membrane to phase separate and vesiculate upon RL action may parallel with protrusions recorded in erythrocytes incubated with di-RL [23]. However, although hemolytic effect has been concomitantly detected [23], no increase in membrane permeability nor membrane rupture/solubilization have been here noticed on model lipid bilayers (GUVs). On the other hand, RL effect might impact significantly the cell signaling by triggering changes in membrane curvature which, by turn, leads to budding mediated by lipids lateral segregation, as observed for some other amphipathic compounds [47]. Ultimately, the alterations promoted by RLs in rafts may have an important effect on di(association) of key proteins thus affecting cell homeostasis, eventually leading to cell death as toxicity side effect.

## Declaration of Competing Interest

The authors declare that they have no known competing financial interests or personal relationships that could have appeared to influence the work reported in this paper.

## CRediT authorship contribution statement

**Benedetta Come:** Investigation. **Maressa Donato:** Investigation. **Lucia Francesca Potenza:** Investigation. **Paolo Mariani:** Conceptualization, Writing- Original draft preparation. **Rosangela Itri:** Conceptualization, Writing- Original draft preparation, Supervision, Funding acquisition. **Francesco Spinozzi:** Conceptualization, Writing- Original draft preparation, Formal analysis, Methodology, Software, Supervision.

## Acknowledgments

425 RI is recipient from Conselho Nacional de Pesquisa (CNPq, Brazil) for research fellowship. FS thank Fabiola Hazizaj and Samuel Pistosini for their extensive use of ImageJ macros.

## Appendix A. Supplementary data

Supplementary data to this article can be found online at ... (file SI.pdf).

## 430 References

- [1] I. C. Ossai, A. Ahmed, A. Hassan, F. S. Hamid, Remediation of soil and water contaminated with petroleum hydrocarbon: A review, *Environmental Technology & Innovation* 17 (2020) 100526.
- [2] M. W. Lim, E. V. Lau, P. E. Poh, A comprehensive guide of remediation technologies for oil contaminated soil — present works and future directions, *Marine Pollution Bulletin* 109 (2016) 14–45.
- [3] R. Boopathy, Factors limiting bioremediation technologies, *Bioresource Technology* 74 (1) (2000) 63 – 67.
- [4] F. L. Martínez, N. B. Moraga, N. Romano-Armada, M. F. Yañez-Yazlle, V. B. Rajal, V. Irazusta, *Stepwise Strategies for the Bioremediation of Contaminated Soils: From the Microbial Isolation to the Final Application*, Springer International Publishing, Cham, 2018, pp. 1–28.
- [5] R. Dixit, Wasiullah, D. Malaviya, K. Pandiyan, U. Singh, A. Sahu, R. Shukla, B. Singh, J. Rai, P. Sharma, et al., Bioremediation of heavy metals from soil and aquatic environment: An overview of principles and criteria of fundamental processes, *Sustainability* 7 (2015) 2189–2212.
- [6] F. Md, Biosurfactant: Production and application, *Journal of Petroleum & Environmental Biotechnology* 3 (2012) 1 – 6.
- [7] K. Muthusamy, S. Gopalakrishnan, T. Ravi, P. Sivachidambaram, Biosurfactants: Properties, commercial production and application, *Current Science* 94 (2008) 736–747.
- [8] D. R. Perinelli, D. Vllasaliu, G. Bonacucina, B. Come, S. Pucciarelli, M. Ricciutelli, M. Cespi, R. Itri, F. Spinozzi, G. F. Palmieri, L. Casettari, Rhamnolipids as epithelial permeability enhancers for macromolecular therapeutics, *European Journal of Pharmaceutics and Biopharmaceutics* 119 (2017) 419 – 425.
- [9] D. E. Otzen, Biosurfactants and surfactants interacting with membranes and proteins: Same but different?, *Biochimica et Biophysica Acta (BBA) - Biomembranes* 1859 (2017) 639 – 649.

- 460 [10] S. J. Varjani, V. N. Upasani, Critical review on biosurfactant analysis, purification and characterization using rhamnolipid as a model biosurfactant, *Bioresource Technology* 232 (2017) 389–397.
- [11] J. L. Parra, J. Guinea, M. A. Manresa, M. Robert, M. E. Mercadé, F. Comelles, M. P. Bosch, Chemical characterization and physicochemical  
465 behavior of biosurfactants, *Journal of the American Oil Chemists Society* 66 (1989) 141–145.
- [12] M. Bustamante, N. Durán, M. C. Diez, Biosurfactants are useful tools for the bioremediation of contaminated soil: a review, *Journal of soil science and plant nutrition* 12 (2012) 667 – 687.
- 470 [13] X. Long, G. Zhang, C. Shen, G. Sun, R. Wang, L. Yin, Q. Meng, Application of rhamnolipid as a novel biodemulsifier for destabilizing waste crude oil, *Bioresource Technology* 131 (2013) 1 – 5.
- [14] K. Mędrzycka, E. Hallmann, S. Pastewski, Evaluation of surfactant and biosurfactant mixture usefulness in oil removal from soil, based on physicochemical studies and flushing experiments, *Environment Protection Engineering* 35 (2015) 191–205.  
475
- [15] L. Santa Anna, G. Sebastian, E. Menezes, T. Alves, A. Santos, N. Pereira Jr., D. Freire, Production of biosurfactants from *Pseudomonas aeruginosa* PA 1 isolated in oil environments, *Brazilian Journal of Chemical Engineering* 19 (2002) 159 – 166.  
480
- [16] G. Soberó-Chávez, F. Lépine, E. Déziel, Production of rhamnolipids by *pseudomonas aeruginosa*, *Applied Microbiology and Biotechnology* 68 (2005) 718–725.
- 485 [17] S. Chong, L. Jiang, H. Shao, C. You, G. Zhang, S. Ding, T. Bian, C. Han, Q. Meng, Targeted killing of myofibroblasts by biosurfactant dirhamnolipid suggests a therapy against scar formation, *Scientific Reports* 6 (2016) 37553.
- [18] H. G. Mortensen, J. K. Madsen, K. K. Andersen, T. Vosegaard, G. R. Deen, D. E. Otzen, J. S. Pedersen, Myoglobin and  $\alpha$ -lactalbumin form smaller complexes with the biosurfactant rhamnolipid than with sds, *Biophysical Journal* 113 (2017) 2621 – 2633.  
490
- [19] M. Sánchez, F. J. Aranda, M. J. Espuny, A. Marqués, J. A. Teruel, A. Manresa, A. Ortiz, Aggregation behaviour of a dirhamnolipid biosurfactant secreted by *pseudomonas aeruginosa* in aqueous media, *Journal of colloid and interface science* 307 (2007) 246—253.  
495
- [20] M. Sánchez, J. A. Teruel, M. J. Espuny, A. Marqués, F. J. Aranda, A. Manresa, A. Ortiz, Modulation of the physical properties of dielaidoylphosphatidylethanolamine membranes by a dirhamnolipid biosurfactant produced by *pseudomonas aeruginosa*, *Chemistry and physics of lipids* 142  
500 (2006) 118–127.

- [21] A. Ortiz, J. A. Teruel, M. J. Espuny, A. Marqués, A. Manresa, F. J. Aranda, Effects of dirhamnolipid on the structural properties of phosphatidylcholine membranes, *International journal of pharmaceutics* 325 (2006) 99–107.
- 505 [22] M. Sánchez, F. J. Aranda, J. A. Teruel, A. Ortiz, Interaction of a bacterial dirhamnolipid with phosphatidylcholine membranes: a biophysical study, *Chemistry and Physics of Lipids* 161 (1) (2009) 51 – 55.
- [23] M. Sánchez, F. J. Aranda, J. A. Teruel, M. J. Espuny, A. Marqués, Ángeles Manresa, A. Ortiz, Permeabilization of biological and artificial membranes by a bacterial dirhamnolipid produced by *pseudomonas aeruginosa*, *Journal of Colloid and Interface Science* 341 (2010) 240 – 247.
- 510 [24] K. Invally, L.-K. Ju, Biolytic effect of rhamnolipid biosurfactant and dodecyl sulfate against phagotrophic alga *ochromonas danica*, *Journal of Surfactants and Detergents* 20 (2017) 1161–1171.
- [25] E. Cammarota, C. Soriani, R. Taub, F. Morgan, J. Sakai, S. L. Veatch, C. E. Bryant, P. Cicuta, Criticality of plasma membrane lipids reflects activation state of macrophage cells, *Journal of The Royal Society Interface* 17 (2020) 20190803.
- 515 [26] K. Simons, E. Ikonen, Functional rafts in cell membranes, *Nature* 387 (1997) 569–572.
- [27] K. Simons, D. Toomre, Lipid rafts and signal transduction, *Nature Reviews Molecular Cell Biology* 1 (2000) 31–39.
- 520 [28] E. Sezgin, I. Levental, S. Mayor, C. Eggeling, The mystery of membrane organization: composition, regulation and roles of lipid rafts, *Nature Reviews Molecular Cell Biology* 18 (2017) 361–374.
- [29] S. L. Veatch, S. L. Keller, Seeing spots: Complex phase behavior in simple membranes, *Biochimica et Biophysica Acta (BBA) - Molecular Cell Research* 1746 (2005) 172 – 185.
- 525 [30] A. G. Ayuyan, F. S. Cohen, Lipid peroxides promote large rafts: effects of excitation of probes in fluorescence microscopy and electrochemical reactions during vesicle formation, *Biophys. J.* 91 (2006) 2172–2183.
- 530 [31] N. F. Morales-Pennington, J. Wu, E. R. Farkas, S. L. Goh, T. M. Konyakhina, J. Y. Zheng, W. W. Webb, G. W. Feigenson, Guv preparation and imaging: Minimizing artifacts, *BBA - Biomembranes* 1798 (2010) 1324–1332.
- [32] C. A. Schneider, W. S. Rasband, K. W. Eliceiri, Nih image to imagej: 25 years of image analysis, *Nature Methods* 9 (2012) 671–675.
- 535 [33] M. Yanagisawa, M. Imai, T. Masui, S. Komura, T. Ohta, Growth dynamics of domains in ternary fluid vesicles, *Biophysical Journal* 92 (2007) 115 – 125.

- 540 [34] R. Lipowsky, Domains and rafts in membranes – hidden dimensions of selforganization, *Journal of Biological Physics* 28 (2002) 195–210.
- [35] B. K. Yoon, J. A. Jackman, M. C. Kim, N.-J. Cho, Spectrum of membrane morphological responses to antibacterial fatty acids and related surfactants, *Langmuir* 31 (2015) 10223–10232.
- 545 [36] T. P. Sudbrack, N. L. Archilha, R. Itri, K. A. Riske, Observing the solubilization of lipid bilayers by detergents with optical microscopy of guvs, *The Journal of Physical Chemistry B* 115 (2011) 269–277.
- [37] B. Mattei, R. B. Lira, K. R. Perez, K. A. Riske, Membrane permeabilization induced by triton x-100: The role of membrane phase state and edge tension, *Chemistry and Physics of Lipids* 202 (2017) 28 – 37.
- 550 [38] P. A. Dalgarno, J. Juan-Colás, G. J. Hedley, L. Piñeiro, M. Novo, C. Perez-Gonzalez, I. D. W. Samuel, M. C. Leake, S. Johnson, W. Al-Soufi, J. C. Penedo, S. D. Quinn, Unveiling the multi-step solubilization mechanism of sub-micron size vesicles by detergents, *Scientific Reports* 9 (2019) 12897.
- 555 [39] B. Come, R. Itri, P. Mariani, F. Spinozzi, In preparation.
- [40] P. I. Kuzmin, S. A. Akimov, Y. A. Chizmadzhev, J. Zimmerberg, F. S. Cohen, Line tension and interaction energies of membrane rafts calculated from lipid splay and tilt, *Biophysical Journal* 88 (2005) 1120–1133.
- [41] G. Staneva, M. Seigneuret, K. Koumanov, G. Trugnan, M. I. Angelova, Detergents induce raft-like domains budding and fission from giant unilamellar heterogeneous vesicles: A direct microscopy observation, *Chemistry and Physics of Lipids* 136 (2005) 55 – 66.
- 560 [42] A. C. Caritá, B. Mattei, C. C. Domingues, E. de Paula, K. A. Riske, Effect of triton x-100 on raft-like lipid mixtures: Phase separation and selective solubilization, *Langmuir* 33 (2017) 7312–7321.
- 565 [43] D. W. Hilgemann, M. Fine, Mechanistic analysis of massive endocytosis in relation to functionally defined surface membrane domains, *Journal of General Physiology* 137 (2011) 155–172.
- [44] O. Maniti, H.-R. Piao, J. Ayala-Sanmartin, Basic cell penetrating peptides induce plasma membrane positive curvature, lipid domain separation and protein redistribution, *The International Journal of Biochemistry & Cell Biology* 50 (2014) 73–81.
- 570 [45] M. Fine, M. C. Llaguno, V. Lariccia, M.-J. Lin, A. Yaradanakul, D. W. Hilgemann, Massive endocytosis driven by lipidic forces originating in the outer plasmalemmal monolayer: a new approach to membrane recycling and lipid domains, *Journal of General Physiology* 137 (2011) 137–154.
- 575

- [46] A. M. Abdel-Mawgoud, F. Lépine, E. Déziel, Rhamnolipids: diversity of structures, microbial origins and roles, *Applied Microbiology and Biotechnology* (2010) 1323–1336.
- 580 [47] D. W. Hilgemann, G. Dai, A. Collins, V. Lariccia, S. Magi, C. Deisl, M. Fine, Lipid signaling to membrane proteins: From second messengers to membrane domains and adapter-free endocytosis, *The Journal of general physiology* 150 (2018) 211–224.

## The Intriguing Role of Rhamnolipids on Plasma Membrane Remodelling: from Lipid Rafts to Membrane Budding

Benedetta Come<sup>1</sup>, Maressa Donato<sup>2,3</sup>, Lucia Francesca Potenza<sup>1</sup>, Paolo Mariani<sup>1</sup>, Rosangela Itri<sup>2\*</sup>,  
Francesco Spinozzi<sup>1\*</sup>

<sup>1</sup> Department of Life and Environmental Sciences, Polytechnic University of Marche, Italy

<sup>2</sup> Institute of Physics, University of São Paulo, Brazil

<sup>3</sup> Center for Laser and Applications, Nuclear and Energy Research Institute, São Paulo, Brazil

\* E-mail: itri@if.usp.br \* E-mail: f.spinozzi@univpm.it

### S1 Determination of the *cmc* of RLs in 0.20 M glucose solutions

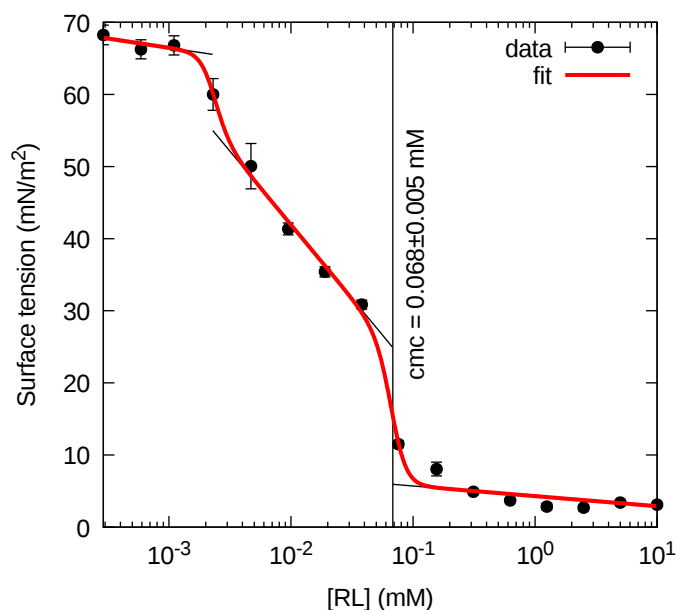


Figure S1: Surface tension of RLs dispersed in 0.20 M glucose solution. The best fit with a combination of three straight lines with two smooth transition described by step functions are shown. The estimation of the *cmc*,  $0.068 \pm 0.005$  mM, has been obtained by the mid point of the second transition, as indicated by the vertical black line.

## S2 Circle passing on a collection of $n$ points

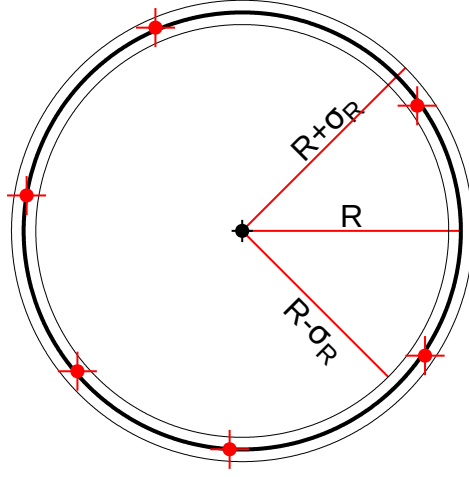


Figure S2: Representation of the best circle passing on six points.

Equations used to calculate the Cartesian coordinates  $x_M$  and  $y_M$  and the radius  $R$  of the optimum circle in the plane that passes on a collection of  $n$  points  $x_i, y_i$ , according to Umbach and Jones<sup>1</sup>

$$x_M = \frac{DC - BE}{AC - B^2} \quad (\text{S1})$$

$$y_M = \frac{AE - BD}{AC - B^2} \quad (\text{S2})$$

where

$$A = nS_{x^2} - S_x^2 \quad (\text{S3})$$

$$B = nS_{xy} - S_x S_y \quad (\text{S4})$$

$$C = nS_{y^2} - S_y^2 \quad (\text{S5})$$

$$D = \frac{1}{2}[nS_{xy^2} - S_x S_{y^2} + nS_{x^3} - S_x S_{x^2}] \quad (\text{S6})$$

$$E = \frac{1}{2}[nS_{yx^2} - S_y S_{x^2} + nS_{y^3} - S_y S_{y^2}] \quad (\text{S7})$$

with

$$S_\alpha = \sum_{i=1}^n \alpha_i \tag{S8}$$

where  $\alpha_i = x_i, y_i, x_i^2, y_i^2, x_i y_i, x_i^3, y_i^3, x_i y_i^2, y_i x_i^2$ . We obtain

$$R = \frac{1}{n} \sum_{i=1}^n \sqrt{(x_i - x_M)^2 + (y_i - y_M)^2} \tag{S9}$$

Equations to find the variances of the center of the circle,  $x_M$  and  $y_M$ , and the circle's radius  $R$

$$\begin{aligned}
\sigma_{x_M}^2 = & \sigma^2(((9S_{y^4} + S_{x^4} + 10S_{x^2y^2})B^6 + (-18S_{y^4} - 2S_{x^4} - 20S_{x^2y^2})AB^4C \\
& + ((10S_{x^2y^2} + 9S_{x^4} + S_{y^4})B^4 + (10S_{x^2y^2} + S_{x^4} + 9S_{y^4})A^2B^2)C^2 \\
& + (-2S_{y^4} - 18S_{x^4} - 20S_{x^2y^2})AB^2C^3 + (S_{y^4} + 9S_{x^4} + 10S_{x^2y^2})A^2C^4 \\
& + (16S_{x^2}C^4 + (16S_{x^2} + 16S_{y^2}2)B^2C^2 + 16S_{y^2}2B^4)D^2 \\
& + (-32S_{x^2}BC^3 + (-16S_{x^2} - 16S_{y^2}2)ABC^2 + (-16S_{x^2} - 16S_{y^2}2)B^3C - 32S_{y^2}2AB^3)DE \\
& + (((4S_{y^2}2 + 4S_{x^2})A^2 + 16S_{x^2}B^2)C^2 + (8S_{x^2} + 8S_{y^2}2)AB^2C \\
& + (4S_{x^2} + 4S_{y^2}2)B^4 + 16S_{y^2}2A^2B^2)E^2)n^2 + ((-12S_{y^2}S_{y^3} \\
& + (-6S_{x^2} - 6S_{xy})S_{y^2}2 - 12S_{x^2y}S_{y^2} + S_{xy}^2 - S_{x^2}^2)B^6 \\
& + (24S_{y^2}S_{y^3} + (12S_{x^2} + 12S_{xy})S_{y^2}2 + 24S_{x^2y}S_{y^2} - 2S_{xy}^2 \\
& + 2S_{x^2}^2)AB^4C + ((-5S_{x^2}^2 - 12S_xS_{x^3} - 4S_{x^2}S_{xy} \\
& + S_{xy}^2 - 12S_xS_{xy^2} + (-2S_{xy} - 2S_{x^2})S_{y^2}2)B^4 + (-S_{x^2}^2 \\
& + S_{xy}^2 - 12S_{x^2y}S_{y^2} + (-6S_{xy} - 6S_{x^2})S_{y^2}2 - 12S_{y^2}S_{y^3})A^2B^2)C^2 \\
& + ((4S_{x^2} + 4S_{xy})S_{y^2}2 + 24S_xS_{xy^2} - 2S_{xy}^2 + 8S_{x^2}S_{xy} \\
& + 24S_xS_{x^3} + 10S_{x^2}^2)AB^2C^3 + ((-2S_{x^2} - 2S_{xy})S_{y^2}2 - 12S_xS_{xy^2} \\
& + S_{xy}^2 - 4S_{x^2}S_{xy} - 12S_xS_{x^3} - 5S_{x^2}^2)A^2C^4 + (-16S_x^2C^4 \\
& + (-16S_x^2 - 16S_{y^2}^2)B^2C^2 - 16S_{y^2}^2B^4)D^2 + (32S_x^2BC^3 \\
& + (16S_x^2 + 16S_{y^2}^2)ABC^2 + (16S_x^2 + 16S_{y^2}^2)B^3C + 32S_{y^2}^2AB^3)DE \\
& + (((-4S_{y^2}^2 - 4S_x^2)A^2 - 16S_x^2B^2)C^2 + (-8S_x^2 - 8S_{y^2}^2)AB^2C \\
& + (-4S_x^2 - 4S_{y^2}^2)B^4 - 16S_{y^2}^2A^2B^2)E^2)n + (8S_x^2S_{x^2} \\
& + 4S_x^2S_{xy} + 4S_x^2S_{y^2}2)A^2C^4 + (-16S_x^2S_{x^2} - 8S_x^2S_{xy} - 8S_x^2S_{y^2}2)AB^2C^3 \\
& + ((4S_{y^2}^2S_{y^2}2 + (8S_{x^2} + 4S_{xy})S_{y^2}^2)A^2B^2 + (4S_x^2S_{y^2}2 \\
& + 4S_x^2S_{xy} + 8S_x^2S_{x^2})B^4)C^2 + ((-8S_{xy} - 16S_{x^2})S_{y^2}^2 - 8S_{y^2}^2S_{y^2}2)AB^4C \\
& + ((4S_{xy} + 8S_{x^2})S_{y^2}^2 + 4S_{y^2}^2S_{y^2}2)B^6)/F
\end{aligned} \tag{S10}$$

$$\begin{aligned}
\sigma_{y_M}^2 = & \sigma^2(((9S_{y^4} + S_{x^4} + 10S_{x^2y^2})A^2B^4 + (S_{y^4} + 9S_{x^4} \\
& + 10S_{x^2y^2})B^6 + ((-20S_{x^2y^2} - 18S_{x^4} - 2S_{y^4})AB^4 + (-20S_{x^2y^2} - 2S_{x^4} - 18S_{y^4})A^3B^2)C \\
& + ((10S_{x^2y^2} + 9S_{x^4} + S_{y^4})A^2B^2 + (10S_{x^2y^2} + S_{x^4} + 9S_{y^4})A^4)C^2 \\
& + (((4S_{y^2}2 + 4S_{x^2})A^2 + 16S_{x^2}B^2)C^2 + (8S_{x^2} + 8S_{y^2}2)AB^2C \\
& + (4S_{x^2} + 4S_{y^2}2)B^4 + 16S_{y^2}2A^2B^2)D^2 + (((-16S_{y^2}2 - 16S_{x^2})A^2B - 32S_{x^2}B^3)C
\end{aligned}$$

where  $\sigma^2$  is the variance in the selection of the  $n$  coordinates  $x_i, y_i$  defining the points.

### S3 Vesicle formed by two sealed spherical caps

Equations for calculating the center-to-center distance  $r_{12}$  and its variance

$$r_{12} = \sqrt{(x_{M,1} - x_{M,2})^2 + (y_{M,1} - y_{M,2})^2} \quad (\text{S14})$$

$$\begin{aligned} \sigma_{r_{12}}^2 = & ((\sigma_{y_{M,1}}^2 + \sigma_{y_{M,2}}^2)y_{M,2}^2 + (-2\sigma_{y_{M,1}}^2 - 2\sigma_{y_{M,2}}^2)y_{M,1}y_{M,2} \\ & + (\sigma_{y_{M,1}}^2 + \sigma_{y_{M,2}}^2)y_{M,1}^2 + (\sigma_{x_{M,1}}^2 + \sigma_{x_{M,2}}^2)x_{M,2}^2 + (-2\sigma_{x_{M,1}}^2 \\ & - 2\sigma_{x_{M,2}}^2)x_{M,1}x_{M,2} + (\sigma_{x_{M,1}}^2 + \sigma_{x_{M,2}}^2)x_{M,1}^2))/r_{12}^2 \end{aligned} \quad (\text{S15})$$

where  $|R_1 - R_2| \leq r_{12} \leq R_1 + R_2$ .

Equations for calculating the standard deviations of the areas  $A_1$  and  $A_2$  and their sum  $A$  of the

spherical caps of radii  $R_1$  and  $R_2$  with center-to-center distance  $r_{12}$  area  $A$  and the volume  $V$

$$\begin{aligned}
\sigma_{A_1}^2 = & \pi^2(9R_1^4r_{12}^2\sigma_{R_1}^2 + 24R_1^3r_{12}^3\sigma_{R_1}^2 \\
& + 22R_1^2r_{12}^4\sigma_{R_1}^2 + 8R_1r_{12}^5\sigma_{R_1}^2 + r_{12}^6\sigma_{R_1}^2 \\
& - 6R_1^2r_{12}^2R_2^2\sigma_{R_1}^2 - 8R_1r_{12}^3R_2^2\sigma_{R_1}^2 - 2r_{12}^4R_2^2\sigma_{R_1}^2 \\
& + r_{12}^2R_2^4\sigma_{R_1}^2 + R_1^6\sigma_{r_{12}}^2 - 2R_1^4r_{12}^2\sigma_{r_{12}}^2 \\
& + R_1^2r_{12}^4\sigma_{r_{12}}^2 - 2R_1^4R_2^2\sigma_{r_{12}}^2 \\
& + 2R_1^2r_{12}^2R_2^2\sigma_{r_{12}}^2 + R_1^2R_2^4\sigma_{r_{12}}^2 + 4R_1^2r_{12}^2R_2^2\sigma_{R_2}^2)/r_{12}^4
\end{aligned} \tag{S16}$$

$$\begin{aligned}
\sigma_{A_2}^2 = & \pi^2(4R_1^2r_{12}^2R_2^2\sigma_{R_1}^2 + R_1^4R_2^2\sigma_{r_{12}}^2 \\
& + 2R_1^2r_{12}^2R_2^2\sigma_{r_{12}}^2 + r_{12}^4R_2^2\sigma_{r_{12}}^2 - 2R_1^2R_2^4\sigma_{r_{12}}^2 - 2r_{12}^2R_2^4\sigma_{r_{12}}^2 \\
& + R_2^6\sigma_{r_{12}}^2 + R_1^4r_{12}^2\sigma_{R_2}^2 - 2R_1^2r_{12}^4\sigma_{R_2}^2 + r_{12}^6\sigma_{R_2}^2 - 8R_1^2r_{12}^3R_2\sigma_{R_2}^2 \\
& + 8r_{12}^5R_2\sigma_{R_2}^2 - 6R_1^2r_{12}^2R_2^2\sigma_{R_2}^2 + 22r_{12}^4R_2^2\sigma_{R_2}^2 \\
& + 24r_{12}^3R_2^3\sigma_{R_2}^2 + 9r_{12}^2R_2^4\sigma_{R_2}^2)/r_{12}^4
\end{aligned} \tag{S17}$$

$$\begin{aligned}
\sigma_A^2 = & (\pi^2(R_1^4r_{12}^2 - 2R_1^2r_{12}^4 + r_{12}^6 + (8r_{12}^5 - 4R_1r_{12}^4 - 8R_1^2r_{12}^3 \\
& + 4R_1^3r_{12}^2)R_2 + (22r_{12}^4 - 16R_1r_{12}^3 - 2R_1^2r_{12}^2)R_2^2 \\
& + (24r_{12}^3 - 12R_1r_{12}^2)R_2^3 + 9r_{12}^2R_2^4)\sigma_{R_2}^2 \\
& + (R_1^6 - 2R_1^4r_{12}^2 + R_1^2r_{12}^4 + (2R_1r_{12}^4 - 2R_1^5)R_2 + (r_{12}^4 \\
& + 4R_1^2r_{12}^2 - R_1^4)R_2^2 + 4R_1^3R_2^3 + ((-2r_{12}^2) \\
& - R_1^2)R_2^4 - 2R_1R_2^5 + R_2^6)\sigma_{r_{12}}^2 + (9R_1^4r_{12}^2 + 24R_1^3r_{12}^3 \\
& + 22R_1^2r_{12}^4 + 8R_1r_{12}^5 + r_{12}^6 \\
& + ((-4R_1r_{12}^4) - 16R_1^2r_{12}^3 - 12R_1^3r_{12}^2)R_2 + ((-2r_{12}^4) - 8R_1r_{12}^3 \\
& - 2R_1^2r_{12}^2)R_2^2 + 4R_1r_{12}^2R_2^3 \\
& + r_{12}^2R_2^4)\sigma_{R_1}^2)/r_{12}^4
\end{aligned} \tag{S18}$$

Standard deviation of the volume encompassed by two spherical caps

$$\begin{aligned}
\sigma_V^2 = & ((\pi^2(R_2 + r_{12} + R_1)^2((16r_{12}^4 - 32R_1r_{12}^3 + 16R_1^2r_{12}^2)R_2^2 \\
& + (32r_{12}^3 - 32R_1r_{12}^2)R_2^3 + 16r_{12}^2R_2^4)\sigma_{R_2}^2 + (R_1^6 - 2R_1^5r_{12} - R_1^4r_{12}^2 \\
& + 4R_1^3r_{12}^3 - R_1^2r_{12}^4 - 2R_1r_{12}^5 \\
& + r_{12}^6 + ((-2r_{12}^5) + 6R_1r_{12}^4 - 4R_1^2r_{12}^3 - 4R_1^3r_{12}^2 + 6R_1^4r_{12} - 2R_1^5)R_2 \\
& + ((-r_{12}^4) - 4R_1r_{12}^3 + 10R_1^2r_{12}^2 - 4R_1^3r_{12} - R_1^4)R_2^2 + (4r_{12}^3 \\
& - 4R_1r_{12}^2 - 4R_1^2r_{12} + 4R_1^3)R_2^3 + ((-r_{12}^2) \\
& + 6R_1r_{12} - R_1^2)R_2^4 + ((-2r_{12}) - 2R_1)R_2^5 + R_2^6)\sigma_{r_{12}}^2 + (16R_1^4r_{12}^2 \\
& + 32R_1^3r_{12}^3 + 16R_1^2r_{12}^4 \\
& + ((-32R_1^2r_{12}^3) - 32R_1^3r_{12}^2)R_2 + 16R_1^2r_{12}^2R_2^2)\sigma_{R_1}^2)/r_{12}^4)/16
\end{aligned} \tag{S19}$$

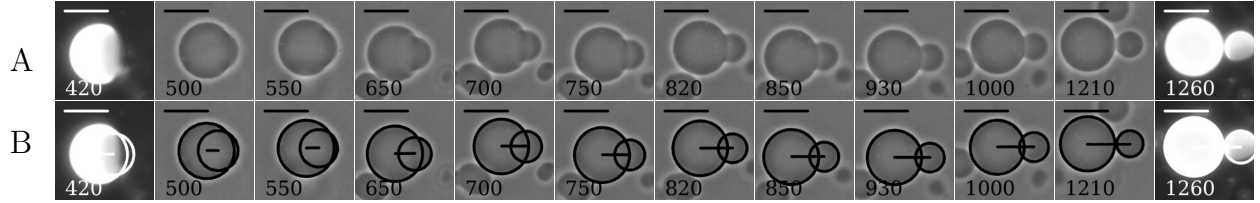


Figure S3: Representative fluorescence images (the first and last ones of each row) and phase contrast images of a second preparation of a GUV composed by DOPC, SM, CHOL (1:1:1) (at 0.00431 mM total lipid concentration) and 0.1 mol % Rho-PE dispersed in a glucose solution containing 0.5 mM RL (panel A). The time sequence, expressed in seconds in the bottom left corner of each image, refers to the elapsed time after mixing RL with GUV solution (considered as time 0 s). The images of panels A with superimposed the best two circles surrounding the GUVs determined with the second ImageJ macro are reported in panel B. All images have been rotated in order to get the line connecting the centres of the two circles (shown in panel B) in the horizontal direction, with the large and the small circle, of radius  $R_1$  and  $R_2$ , on the left and the right side, respectively. The distance  $r_{12}$  (Eq. 5) between the centres is shown as black or a white line. The top right bars span 20  $\mu\text{m}$ .

#### S4 Rate of $L_o$ - $L_d$ GUV:RL interaction

We assume that the bilayer of the GUV is a combination of a  $L_o$  domain, containing a number  $N_{L_o}$  of lipid molecules forming the ordered phase (SM and CHOL in our case) and a  $L_d$  domain with  $N_{L_d}$  lipid molecules forming the disordered phase (DOPC in our case). The ratio  $\phi = \frac{N_{L_o}}{N_{L_d}}$  is fixed by the composition of the GUV ( $\phi = 2$  in case of 1:1:1 DOPC, SM, CHOL). Corresponding

average areas per polar head are  $a_{L_o}$  and  $a_{L_d}$ , respectively (in our case  $a_{L_o} = \frac{1}{2}(a_{SM} + a_{CHOL})$  and  $a_{L_d} = a_{DOPC}$ ).

We also assume that at the time  $t$  a number  $N_{RL,d}$  of RL molecules are located in the outer leaflet of the  $L_d$  domain and a number  $N_{RL,o}$  of them are placed in the outer leaflet of the  $L_o$  domain. We make the approximation that each RL molecule increases the outer leaflet surface of  $L_d$  or  $L_o$  domain by the same average area  $a_{RL}$ . The maximum possible values of the numbers of RL inserted in the outer leaflets, called  $N_{RL,d}^0$  and  $N_{RL,o}^0$ , will be dictated by the sample composition, namely by the ratios  $\zeta_d = \frac{[RL]}{[L_d]}$  and  $\zeta_o = \frac{[RL]}{[L_o]}$  (with  $[L_o] = \phi[L_d]$ ), according to

$$N_{RL,d}^0 = \zeta_d N_{L_d} \quad (S20)$$

$$N_{RL,o}^0 = \zeta_o N_{L_o} \quad (S21)$$

In our case, being the total lipid concentration  $C = 3[L_d] = 0.00431$  mM, we have  $\zeta_d = 2\zeta_o = 139$  at 0.2 mM RL and  $\zeta_d = 2\zeta_o = 348$  at 0.5 mM RL.

According to our results (see Fig. 6, panels D-E), the time evolution of  $L_d$  and  $L_o$  surfaces of the GUV can be approximated by straight lines,

$$A_1 = A_{1,0} + m_{A_1} t \quad (S22)$$

$$A_2 = A_{2,0} + m_{A_2} t \quad (S23)$$

On this basis,  $L_d$  and  $L_o$  surfaces as a function of time are

$$A_1 = a_{L_d} \frac{N_{L_d}}{2} + a_{RL} N_{RL,d} \quad (S24)$$

$$A_2 = a_{L_o} \frac{N_{L_o}}{2} + a_{RL} N_{RL,o} \quad (S25)$$

At  $t = 0$  there is not RL in solution ( $N_{RL,d} = N_{RL,o} = 0$ ), hence

$$A_{1,0} = a_{L_d} \frac{N_{L_d}}{2} \quad (S26)$$

$$A_{2,0} = a_{L_o} \frac{N_{L_o}}{2} \quad (S27)$$

so that

$$N_{L_d} = \frac{2A_{1,0}}{a_{L_d}} \quad (S28)$$

$$N_{L_o} = \frac{2A_{2,0}}{a_{L_o}} \quad (S29)$$

Combining Eqs. S22-S23 and S24-S25, we obtain

$$N_{RL,d} = \frac{m_{A_1} t}{a_{RL}} \quad (S30)$$

$$N_{RL,o} = \frac{m_{A_2} t}{a_{RL}} \quad (S31)$$

The time evolution of the interaction of RL molecules with lipid molecules in  $L_d$  and  $L_o$  domain will be described by the ratios

$$\frac{N_{RL,d}}{N_{L_d}} = \frac{m_{A_1} a_{L_d} t}{2A_{1,0} a_{RL}} \quad (S32)$$

$$\frac{N_{RL,o}}{N_{L_o}} = \frac{m_{A_2} a_{L_o} t}{2A_{2,0} a_{RL}} \quad (S33)$$

We can also find out the time evolution of fraction of RL molecules with respect the total RL available molecules that interact with  $L_d$  or  $L_o$  domains,

$$f_d = \frac{N_{RL,d}}{N_{RL,d}^0} = \frac{m_{A_1} a_{L_d} t}{2\zeta_d A_{1,0} a_{RL}} \quad (S34)$$

$$f_o = \frac{N_{RL,o}}{N_{RL,o}^0} = \frac{m_{A_2} a_{L_o} t}{2\zeta_o A_{2,0} a_{RL}} \quad (S35)$$

As a result, we obtain that the rates of the fractions of RL molecules in respect to the total RL concentration interacting with  $L_d$  or  $L_o$ , respectively, are given by the following expressions, both independent on time,

$$\gamma_d = \frac{m_{A_1} a_{L_d}}{2\zeta_d A_{1,0} a_{RL}} \quad (S36)$$

$$\gamma_o = \frac{m_{A_2} a_{L_o}}{2\zeta_o A_{2,0} a_{RL}} \quad (S37)$$

## References

- [1] D. Umbach, K. N. Jones, A few methods for fitting circles to data, IEEE Transactions on Instrumentation and Measurement 52 (2003) 1881–1885.